

ORIGINAL RESEARCH

Open Access



Improved voltage tracking of autonomous microgrid technology using a combined resonant controller with lead-lag compensator adopting negative imaginary theorem

Md. Yah-Ya Ul Haque^{1,2*} , Md. Rashidul Islam² , Tanvir Ahmed² and Md. Rafiqul Islam Sheikh²

Abstract

Growing application of distributed generation units at remote places has led to the evolution of microgrid (MG) technology. When an MG system functions independently, i.e., in autonomous mode, unpredictable loads and uncertainties emerge throughout the system. To obtain stable and flexible operation of an autonomous MG, a rigid control mechanism is needed. In this paper, a robust high-performance controller is introduced to improve the performance of voltage tracking of an MG system and to eliminate stability problems. A combination of a resonant controller and a lead-lag compensator in a positive position feedback path is designed, one which obeys the negative imaginary (NI) theorem, for both single-phase and three-phase autonomous MG systems. The controller has excellent tracking performance. This is investigated through considering various uncertainties with different load dynamics. The feasibility and effectiveness of the controller are also determined with a comparative analysis with some well-known controllers, such as linear quadratic regulator, model predictive and NI approached resonant controllers. This confirms the superiority of the designed controller.

Keywords: Negative imaginary theorem, Resonant controller, Lead-lag compensator, Autonomous microgrid, Voltage tracking

1 Introduction

Consumption of electrical energy is increasing rapidly, following the rapid growth of the world's population. To meet the demand, largely fossil fuels have been used. However, fossil fuels pollute the environment. At the same time, they are also depleting dramatically [1, 2]. To overcome this problem, renewable energy is one of the prime solutions, and different renewable energy generating units such as wind turbine, photovoltaic (PV), hydro, bio-mass, hydrogen fuel cells have been considered as distributed generator (DG) units located at customer

sites [3, 4]. These DGs are connected to the utility grid through microgrid (MG) systems. Furthermore, the MG contains various loads including linear and nonlinear, balanced and unbalanced, static and dynamic types, as well as lines and distribution transformers, and energy storage systems (ESS) [5–7]. It is also worth noting that DG units cannot provide accurate 50/60 Hz power supply to the MG owing to their characteristics. To interface an MG with DG units, voltage source inverters (VSI) are used, and thus, to obtain the quality voltage and power outputs, VSI control is extremely important [8]. A simple MG structure with some conventional DG units, VSI and loads is depicted in Fig. 1.

An MG must have the ability to accommodate any uncertainty and abnormality, and bring the system back into an equilibrium position within the shortest possible

*Correspondence: yahyahaque133@gmail.com

¹ Department of Electrical and Electronic Engineering, Varendra University, Rajshahi 6204, Bangladesh
Full list of author information is available at the end of the article

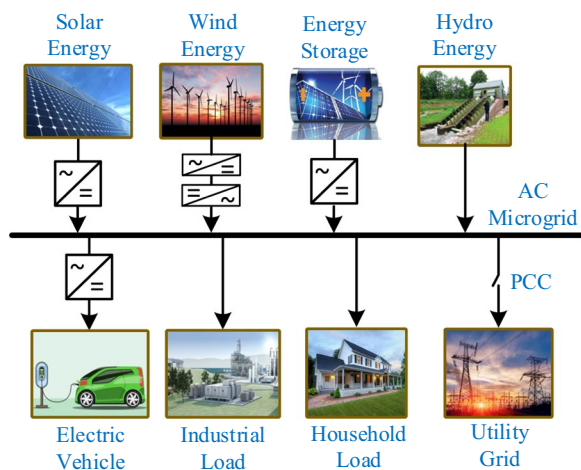


Fig. 1 Microgrid configuration

time after a disturbance. The functions of an MG can be segmented into non-isolated (grid connected) mode and isolated (autonomous) mode [9]. In non-isolated mode, the utility grid controls the voltage and frequency of the MG, and the MG is treated as a controllable generator or load. In the case of autonomous mode, the MG itself has to control the different parameters including voltage, frequency, active and reactive power, power-factor etc. Thus, a robust control system is necessary for satisfactory operation of an autonomous MG.

Research has made significant progress on MG controlling technology for maintaining good performance. The linear quadratic regulator (LQR) [10, 11], integral-LQR (I-LQR) [12], linear quadratic Gaussian (LQG) [13], and integral-LQG (I-LQG) [14] are well-known controllers based on linearization techniques. These have been proposed for the voltage control of an MG. Accurate voltage tracking is the main advantage of these controllers, but the dynamics of these controllers depend on the dynamics of the plant and their performance degrades if the plant changes. Furthermore, according to the order of the plant dynamics, the order of the controller also increases. Proportional integral derivative (PID) [15] and proportional integral (PI) [16] controllers are very common and widely used for voltage and power control of an MG because of their simplicity and easy implementation. However, during disturbances, their performance degrades and steady-state errors occur because of the unbalanced system. In addition, if the operating point changes, the performance of the controllers is also hampered.

Decentralized and distributed control strategies [17–19] are two more control systems frequently used in an MG to compensate for deviations in frequency and voltage. These controllers require parameters which are

measured by remote sensing blocks and sent back to the controller through low bandwidth communication systems. Thus, the low bandwidth and slow control loop are the principal drawbacks of these controllers.

An H-infinity controller [20, 21] has been proposed to acquire good stabilization with guaranteed performance of an MG. However, the order of the system is a big issue for such a controller and advanced digital signal processing (DSP) is required for satisfactory performance. In addition, high mathematical understanding is needed for modeling this controller, while its slow dynamic response restricts its use. The hierarchical control technique [22, 23] which is another well-known controller, is commonly used in a power system to control voltage and frequency. Three different levels are required, where each level is assigned to perform a distinctive control action. If one of the control levels collapses, the whole control system fails.

Model predictive control (MPC) [24, 25] is an advanced control technique extensively used to control an MG system while satisfying some constraints. Lower switching frequency and accurate voltage control with lower total harmonic distortion (THD) are the main advantages of this controller. However, sensitivity to parameter variations, as well as the need for an advanced DSP system to implement the higher order system are its major limitations. The hysteresis controller, which is another control technique based on the current controlled pulse width modulation (PWM) technique proposed in [26, 27], has fast transient response and low complexity in design. However, the considerable amount of ripple in current and variation of switching frequency limit its use at large scale. The repetitive controller [28, 29] is also a good competitor for voltage control of an MG. It is designed to eliminate periodic disturbance and minimize harmonics in the system. However, it is difficult to stabilize the controller against all unknown load disturbances, and it responds sluggishly while loads fluctuate.

In order to damp out the resonant mode in a power system, different damping controllers have been proposed, such as the proportional resonant (P-RC) [30, 31] and proportional integral resonant controllers (PI-RC) [32]. These improve the performance of the MG. These controllers are simple in structure, and can efficiently control selective harmonics and show negligible steady-state error. However, they are extremely sensitive to frequency variation and require accurate tuning. Negative imaginary (NI) based-resonant (NI-R) [33], proportional resonant [34] and proportional plus lead compensator controllers [35] also promote voltage tracking performance along with damping resonant peak in islanded MG system, and exhibit robust performance against different load dynamics. However, they show poor

performance in minimizing transient oscillation in some cases, and also the magnitude and phase errors in voltage tracking degrade their performance.

The above descriptions demonstrate the need for further improvements in voltage control of an MG system for precise reference tracking. Therefore, in this paper, a robust high-performance controller is designed to amend voltage tracking performance against various uncertainties and different loads in autonomous MG technology for both single-phase and three-phase systems. The designed controller is modeled with a resonant (R) controller, series connected with a lead-lag compensator (LLC), which obeys the NI theorem for guaranteeing system stability, abbreviated to ‘NI-RLLC’ controller. The NI-RLLC controller rigorously eliminates the drawbacks mentioned above, and has the advantages of both the resonant controller and lead-lag compensator. The lead compensator shifts the root locus to the left for achieving good transient stability, while steady state errors in phase and magnitude are minimized through the lag compensator. The pole and zero of the lag compensator are placed near the origin and close to each other to avoid the instability problem. The main focus of the proposed work is to control the output voltage to track the reference to ensure the lowest magnitude and phase errors as well as THD, considering different uncertainties, nonlinearities and unknown dynamics of loads. To prove the superiority of the designed NI-RLLC controller, its performance is compared with the well-known LQR, MPC and NI-R controllers. The controller and the system are simulated through MATLAB software.

The rest of the paper is structured as follows. Section 2 describes MG modeling while Sect. 3 presents the design procedure of the NI-RLLC controller. Comparison of controllers is discussed in Sect. 4 and the performance of the controller is evaluated in Sect. 5. Section 6 concludes the paper.

2 Modeling of autonomous MG technology

The configuration and modelling of single-phase and three-phase autonomous MGs are provided in this section.

2.1 Autonomous MG configuration

An MG mainly consists of three essential elements: an input energy source, an energy conversion unit and a filter. A single-phase MG system with these elements is shown in Fig. 2a. For modeling purposes, a DC voltage source is used as the source for generating power, and an IGBT-based full bridge VSI is used to convert the DC voltage into AC. In order to eliminate high frequency harmonic components from the VSI output, a filter consisting of inductor and capacitor is used after the VSI. As the MG system operates at low voltage with short lines, only the series resistance is considered here as line impedance [36]. Figure 2b depicts the three-phase MG system, where a three-phase VSI and a filter are used to regulate voltage and current. Additionally, the three-phase MG has step-up transformer, point of common coupling (PCC) and loads, where loads are connected to the high voltage side of the transformer at PCC [37].

Figure 2a, b also show the closed-loop control structures of single-phase and three-phase MG systems, respectively. Measured output voltages and reference voltages are injected to the controllers as shown in Fig. 2a, b. Necessary actions are imposed to generate proper control signals which are sent to the PWM blocks to control the IGBT switches.

2.2 Mathematical modeling of single-phase MG system

In this subsection, a state space mathematical model is provided for the autonomous MG technology as shown in Fig. 2a. Considering \hat{V}_L as the voltage across inductor L_s , and \hat{I}_L as inductor current, there is [38, 39]:

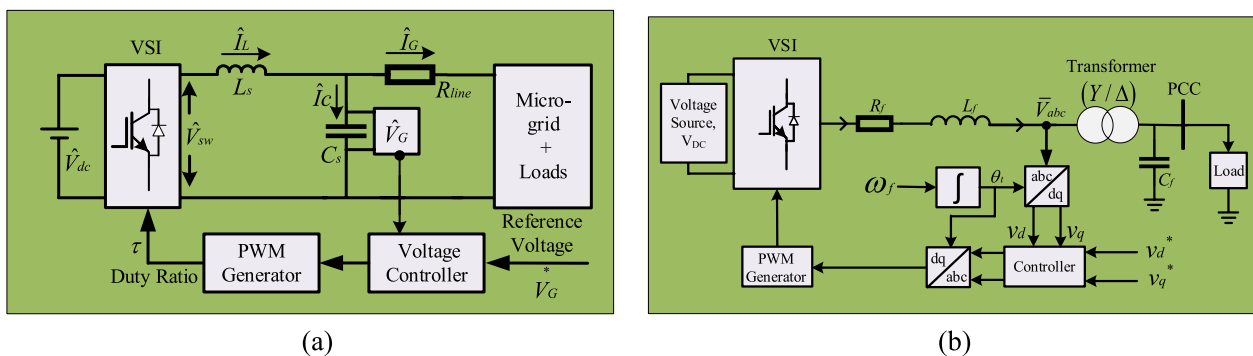


Fig. 2 Closed-loop configuration of MG technology for a single-phase system and b three-phase system

$$\hat{V}_L = L_s \frac{d\hat{I}_L}{dt} \tag{1}$$

Applying KVL yields:

$$\hat{V}_{sw} = \hat{V}_L + \hat{V}_G \tag{2}$$

Substituting (1) into (2) yields:

$$\frac{d\hat{I}_L}{dt} = \frac{\hat{V}_L}{L_s} = \frac{\hat{V}_{sw} - \hat{V}_G}{L_s} \tag{3}$$

where \hat{V}_{sw} and \hat{V}_G represent input voltage and output voltage, respectively. $\hat{V}_{sw} = \tau \hat{V}_{DC}$ is the average switching voltage and duty ratio $\tau \in \{-1, 1\}$.

Considering \hat{I}_C as the current through the capacitor and \hat{V}_G the capacitor voltage, there is:

$$\hat{I}_C = C_s \frac{d\hat{V}_G}{dt} \tag{4}$$

Using KCL obtains:

$$\hat{I}_L = \hat{I}_C + \hat{I}_G \tag{5}$$

Substituting (4) into (5) yields:

$$\frac{d\hat{V}_G}{dt} = \frac{\hat{I}_C}{C_s} = \frac{\hat{I}_L - \hat{I}_G}{C_s} \tag{6}$$

Equations (3) and (6) can be represented in the time-domain as:

$$\frac{d}{dt} \begin{bmatrix} \hat{I}_L \\ \hat{V}_G \end{bmatrix} = \begin{bmatrix} 0 & -\frac{1}{L_s} \\ \frac{1}{C_s} & 0 \end{bmatrix} \begin{bmatrix} \hat{I}_L \\ \hat{V}_G \end{bmatrix} + \begin{bmatrix} \frac{1}{L_s} \\ 0 \end{bmatrix} \hat{V}_{sw} + \begin{bmatrix} 0 \\ -\frac{1}{C_s} \end{bmatrix} \hat{I}_G \tag{7}$$

Loads in MG are considered as black box as they change randomly and abruptly, and thus, \hat{I}_G in (7) is treated as disturbance. As the purpose is to follow the reference voltage properly, \hat{V}_G is considered as output, i.e.:

$$y = [\hat{V}_G] = [0 \ 1] \begin{bmatrix} \hat{I}_L \\ \hat{V}_G \end{bmatrix} \tag{8}$$

Considering (7) and (8), the general form of the system in the Laplace domain can be written as [40]:

$$W(s) = W_0(s) + \Delta_t(s) \tag{9}$$

where $W_0(s) = C_t(sI - A_t)^{-1}B_t + D_t$ is the plant transfer function, and $\Delta_t(s) = \begin{bmatrix} 0 \\ -\frac{1}{C_s} \end{bmatrix} \hat{I}_G(s)$ is the output to input

uncertainty. Also, the system matrix is $A_t = \begin{bmatrix} 0 & -\frac{1}{L_s} \\ \frac{1}{C_s} & 0 \end{bmatrix}$,

the input matrix $B_t = \begin{bmatrix} \frac{1}{L_s} \\ 0 \end{bmatrix}$; the output matrix

$C_t = [0 \ 1]$, and the feed-through matrix $D_t = 0$. The required parameters of the single-phase MG system are listed in Table 1.

2.3 Mathematical modeling of three-phase MG system

Mathematical analysis of the three-phase MG system is constructed with the aid of Fig. 2b. The dynamical equation of the topology in the *abc*-frame can be expressed as [41, 42]:

$$\bar{I}_{t,abc} = C_f \frac{d\bar{V}_{abc}}{dt} \tag{10}$$

$$\bar{V}_{t,abc} = L_f \frac{d\bar{I}_{t,abc}}{dt} + R_f \bar{I}_{t,abc} + \bar{V}_{abc} \tag{11}$$

In (10) and (11), $\bar{V}_{t,abc}$, $\bar{I}_{t,abc}$ and \bar{V}_{abc} are 3×1 matrices consisting of independent phase quantity in the time-domain. Rearranging (10) and (11) leads to:

$$\frac{d\bar{V}_{abc}}{dt} = \frac{1}{C_f} \bar{I}_{t,abc} \tag{12}$$

$$\frac{d\bar{I}_{t,abc}}{dt} = \frac{1}{L_f} \bar{V}_{t,abc} - \frac{R_f}{L_f} \bar{I}_{t,abc} - \frac{1}{L_f} \bar{V}_{abc} \tag{13}$$

Assuming balanced DG units and loads, Eqs. (12) and (13) can be transformed into a rotating *dq*-frame using the Park transformation as:

$$\frac{d\bar{V}_{dq}}{dt} = \frac{1}{C_f} \bar{I}_{t,dq} - j\omega_f \bar{V}_{dq} \tag{14}$$

$$\frac{d\bar{I}_{t,dq}}{dt} = \frac{1}{L_f} \bar{V}_{t,dq} - \frac{R_f}{L_f} \bar{I}_{t,dq} - \frac{1}{L_f} \bar{V}_{dq} - j\omega_f \bar{I}_{t,dq} \tag{15}$$

Equations (14) and (15) consist of components in the *d*- and *q*-axes, where the *d*- and *q*-axes represent real and imaginary parts, respectively. Dissociating these two components, Eqs. (14) and (15) are formed as:

$$\frac{d\bar{V}_d}{dt} = \frac{1}{C_f} \bar{I}_{t,d} + \omega_f \bar{V}_q \tag{16}$$

$$\frac{d\bar{V}_q}{dt} = \frac{1}{C_f} \bar{I}_{t,q} - \omega_f \bar{V}_d \tag{17}$$

$$\frac{d\bar{I}_{t,d}}{dt} = \frac{1}{L_f} \bar{V}_{t,d} - \frac{R_f}{L_f} \bar{I}_{t,d} - \frac{1}{L_f} \bar{V}_d + \omega_f \bar{I}_{t,q} \tag{18}$$

Table 1 Parameters of single-phase MG

Parameters	DC voltage source, \bar{V}_{DC}	Switching frequency, f_s	Fundamental frequency, f_0	Inductance of filter, L_s	Capacitance of filter, C_s	Line resistance, R_{line}	Load resistance, R_{Load}
Value	250 V	6000 Hz	50 Hz	1.5 mH	18 μ F	0.40 Ω	35 Ω

$$\frac{d\bar{I}_{t,q}}{dt} = \frac{1}{L_f} \bar{V}_{t,q} - \frac{R_f}{L_f} \bar{I}_{t,q} - \frac{1}{L_f} \bar{V}_q + \omega_f \bar{I}_{t,d}. \quad (19)$$

The standard state space equations of the MG system can be expressed as:

$$\dot{x}(t) = A_m x(t) + B_m u(t) \quad y(t) = C_m x(t) + D_m u(t) \quad (20)$$

where, $A_m = \begin{bmatrix} 0 & \omega_f & \frac{1}{C_f} & 0 \\ -\omega_f & 0 & 0 & \frac{1}{C_f} \\ -\frac{1}{L_f} & 0 & -\frac{R_f}{L_f} & \omega_f \\ 0 & -\frac{1}{L_f} & \omega_f & -\frac{R_f}{L_f} \end{bmatrix}$, $B_m = \begin{bmatrix} 0 & 0 \\ 0 & 0 \\ \frac{1}{L_f} & 0 \\ 0 & \frac{1}{L_f} \end{bmatrix}$,

$C_m = \begin{bmatrix} 1 & 0 & 0 & 0 \\ 0 & 1 & 0 & 0 \end{bmatrix}$ and $D_m = 0$. Also, the state vectors are $x(t) = [\bar{V}_d \ \bar{V}_q \ \bar{I}_{t,d} \ \bar{I}_{t,q}]^T$, the input or control vectors are $u(t) = [\bar{V}_{t,d} \ \bar{V}_{t,q}]^T$, and the output vectors are $y(t) = [\bar{V}_d \ \bar{V}_q]$.

To design an MIMO control system for a three-phase MG in the s -domain, illustrated in Fig. 3a, the nominal plant transfer function is obtained from (20), thus:

$$W_m(s) = C_m(sI - A_m)^{-1} B_m + D_m$$

Table 2 lists the necessary parameters required for the three-phase MG system.

3 Controller design for single-phase and three-phase autonomous MG systems

3.1 Controller design for single-phase MG system

Figure 3a shows the block diagram of the closed-loop control structure for an autonomous MG system. Here, the reference signal is defined as $R(s)$ and the output signal is $Y(s)$. For a single-phase system, $W(s)$ represents the nominal plant transfer function between input voltage \hat{V}_{sw} and output voltage \hat{V}_G , $H(s)$ is the resonant controller and $C(s)$ is the lead-lag compensator. For robust performance, the feedback compensator $C(s)$ is connected in series with the resonant controller $H(s)$. The transfer function of the resonant controller $H(s)$ for a simple single input single output (SISO) system can be expressed as [33, 43, 44]:

$$H(s) = -k_s \frac{s(s + 2\xi_s \omega_s)}{s^2 + 2\xi_s \omega_s s + \omega_s^2} \quad (21)$$

where k_s is the resonant gain of the controller, ξ_s is the damping co-efficient, and ω_s is the resonant frequency. For proper stabilization of this controller, all its parameters are higher than zero. The optimized value of ξ_s is taken, as a large value leads to low damping while a small value provides unwanted phase shift. The closed-loop transfer function of the system $W(s)$ associating with the resonant controller $H(s)$ can be expressed as:

$$\hat{W}_{Cl}(s) = \frac{W(s)}{1 - W(s) * H(s)} \quad (22)$$

This resonant controller $H(s)$ is designed by the NI theorem (NI-R) [33], which is a simple second order controller. However, this controller has steady-state phase and amplitude errors, and also shows poor performance in transient condition with considerable oscillations.

To alleviate these drawbacks, a lead-lag compensator $C(s)$ is cascaded in series with the resonant controller $H(s)$, i.e., RLLC controller, for better and robust performance. The RLLC controller is designed to satisfy the NI theorem, and is thus called NI-RLLC. According to the NI theorem [43, 45], the positive feedback interconnection of two NI systems will be stable if one of the systems is strictly negative imaginary (SNI) and the DC loop gain remains less than unity. From Fig. 3b, it is clear that the phase of the plant transfer function $W(s)$ lies within -180° and 0° , which implies that the system is an NI system. The transfer function of the lead-lag compensator $C(s)$ with a gain k_c can be written as [46, 47]:

$$C(s) = k_c \frac{(s + z_{s1})(s + z_{s2})}{(s + p_{s1})(s + p_{s2})} \quad (23)$$

The zero and pole of the lead compensator are denoted by z_{s1} and p_{s1} , respectively, and $|p_{s1}| > |z_{s1}|$. For the lag compensator, z_{s2} and p_{s2} are the zero and pole, respectively, and $|z_{s2}| > |p_{s2}|$. The values of the parameters are chosen as $k_c = 3.5$, $z_{s1} = 4100$, $p_{s1} = 9600$, $z_{s2} = 4$ and $p_{s2} = 3$. The overall closed-loop transfer function with the designed NI-RLLC controller can be written as:

$$W_{Cl}(s) = \frac{W(s)}{1 - W(s) * F(s)} \quad (24)$$

where $F(s) = H(s) * C(s)$.

Figure 3b shows that the loop gain $W(s) * F(s)$ is still less than unity at low frequency which stabilizes the

designed controller. Nyquist and root-locus plots are depicted in Fig. 4a, b, respectively. It can be seen that the stability criterion of the designed NI-RLLC controller is guaranteed, as no root is located in the right-half plane. The performance of the designed NI-RLLC controller is examined through imposing different uncertainties and various load dynamics. Different parameters of the SISO NI-RLLC controller are listed in Table 3.

3.2 Controller design for three-phase MG system

Designing a multiple input multiple output (MIMO) controller is much more challenging as multiple subsystems may consist of a number of power sources in each subsystem, while the numbers of control inputs and outputs increase. The closed-loop control technique for three-phase MG technology is shown in Figs. 2b and 3a, where $\bar{V}_{t,d}$ and $\bar{V}_{t,q}$ are the two control inputs, and \bar{V}_d , \bar{V}_q are the two output signals to be controlled. The transfer function matrix of the MIMO closed-loop system for plant $W_m(s)$ and controller $F_m(s)$ can be formed as:

$$W_{mCl}(s) = \frac{W_m(s)}{1 - W_m(s) * F_m(s)} \tag{25}$$

where $F_m(s) = H_m(s) * C_m(s)$.

For the MIMO system, $H_m(s)$ and $C_m(s)$ can be provided in the following way:

$$H_m(s) = -k_m \frac{s(s + 2\xi_m\omega_m)}{s^2 + 2\xi_m\omega_m s + \omega_m^2} \beta_{m \times m} \tag{26}$$

$$C_m(s) = k_p \frac{(s + z_{m1})(s + z_{m2})}{(s + p_{m1})(s + p_{m2})} \eta_{m \times m} \tag{27}$$

$\beta_{m \times m}$ and $\eta_{m \times m}$ are square matrices of order 2×2 for a two-state MG system. The compensator gains are chosen as: $k_p = 2$, $z_{m1} = 3800$, $p_{m1} = 8600$, $z_{m2} = 4$ and $p_{m2} = 3$. The values of various parameters are listed in Table 4. For better perception of the control mechanism, a flowchart is given in Fig. 5 for the MIMO NI-RLLC controller. In the case of the SISO system, $\beta_{m \times m}$ and $\eta_{m \times m}$ are 1×1 matrices, and there is no need to dissociate the input voltage. However, the rest of the procedure is identical for the two systems. Since the objective is to control the voltage of the autonomous MG system, the corresponding load voltages of the SISO and MIMO systems are considered as inputs, and the outputs of the control systems are the regulated PWM signals for the inverter IGBTs.

4 Comparative study of controllers

To evaluate the superior performance of the designed NI-RLLC controller, time-domain and frequency-domain comparisons are displayed in Figs. 6 and 7, respectively,

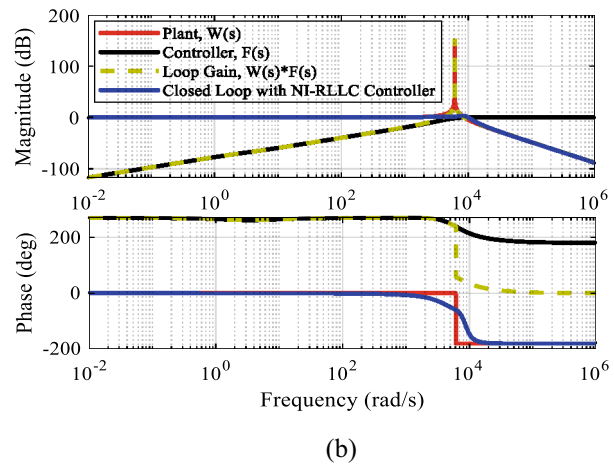
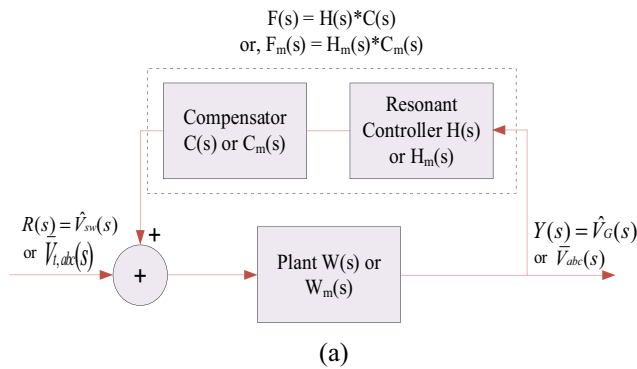


Fig. 3 a Closed-loop control structure of MG system both for single-phase and three-phase b bode plot of different transfer functions for single-phase

Table 2 Parameters of three-phase MG

Parameters	DC bus voltage, V_{DC}	VSI terminal voltage, V_{base}	Voltage ratio of transformer, Y/Δ	DG rated power, S_{base}	Switching frequency, f_s	Fundamental frequency, f_0	Resistance of filter, R_f	Inductance of filter, L_f	Capacitance of filter, C_f
Value	2000 V	600 V 1 (pu)	0.6 kV/13.8 kV	3 MVA 1 (pu)	1980 Hz	50 Hz	2.5 mΩ	90 μH	105 μF

for single-phase and three-phase systems. Commonly used controllers, including LQR and MPC together with NI-R controller are considered for comparison. The design procedure of LQR, MPC, and NI-R is adopted from [33, 48, 49], respectively. For fair comparison, the resonant controller parameters of the NI-R controller and the designed NI-RLLC controller are kept the same as shown in Tables 3 and 4, respectively. The required parameters of the LQR controller are chosen as follows:

$$\text{SISO LQR: } Q_s = \begin{bmatrix} 10 & 0 \\ 0 & 10^{-2} \end{bmatrix} \text{ and } R_s = 14.$$

$$\text{MIMO LQR: } Q_m = \begin{bmatrix} 2 & 0 & 0 & 0 \\ 0 & 3 & 0 & 0 \\ 0 & 0 & 5 & 0 \\ 0 & 0 & 0 & 3 \end{bmatrix} \text{ and } R_m = \begin{bmatrix} 300 & 0 \\ 0 & 350 \end{bmatrix}.$$

For the SISO MPC controller, the prediction horizon and control horizon are selected as 10 and 1, respectively, and the weights are chosen as 0.1 and 11. Prediction and control horizons are kept unchanged whereas weights are selected as {0.1, 0.1} and {13, 200} for MIMO MPC.

Numerical values of different terms for different controllers which represent the step responses for single-phase and three-phase systems are listed in Tables 5 and 6, respectively. It is clear from the tables that the designed NI-RLLC controller for both SISO and MIMO systems achieves outstanding performance. The step response of the closed-loop system using the designed SISO NI-RLLC controller approaches steady-state with null offset, nearly 76.39%, 86.92% and 77.63% faster than the NI-R controller, LQR and MPC, respectively. Incorporating rapid rise time and peak time, the designed NI-RLLC controller reduces the overshoot by around 54.35%, 67.31% and 59.41% with respect to the NI-R controller,

performance is obtained for the three-phase system, with lower percentage of overshoot, faster rise time and peak time, as well as lower settling time with zero steady-state error. Obviously, these relative analyses prove that the designed NI-RLLC controller is more reliable than the other controllers in all aspects for voltage tracking of an autonomous MG system.

5 Performance evaluation for single-phase autonomous MG system

5.1 Performance over different uncertainties

Uncertainties in a system arise on account of unknown load parameters, unmodeled load dynamics, load variation etc. In order to achieve robust performance, a controller must perform sensitively under various uncertainties. For robust analysis of the designed NI-RLLC controller, multiplicative input uncertainty, inverse additive uncertainty and inverse multiplicative input uncertainty are imposed on the plant, whose block diagrams are depicted in Fig. 8a–c, respectively, where $W_0(s)$, E_0 and $\Delta_t(s)$ represent plant transfer function, scalar weights and plant variation, respectively. The values of E_0 and $\Delta_t(s)$ are selected by considering 25% of reference amplitudes as plant variation. Effectiveness of the controller against all the uncertainties is shown in Fig. 8d–f. It is clear that the open-loop responses become severely distorted because of plant variation, whereas the NI-R

Table 3 Parameters of SISO NI-RLLC controller

Quantity	Value
Resonant gain, k_s	0.3
Resonant damping co-efficient, ζ_s	0.7
Resonant frequency, ω_s	6080

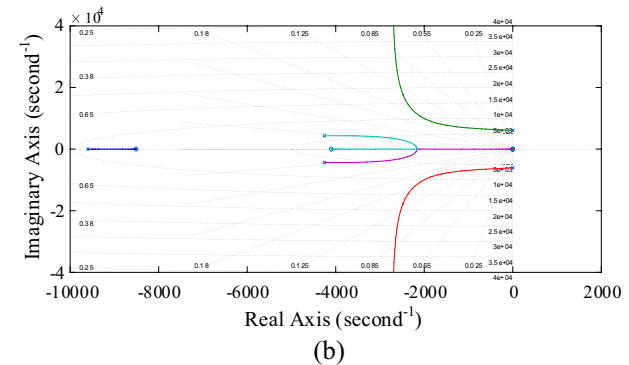
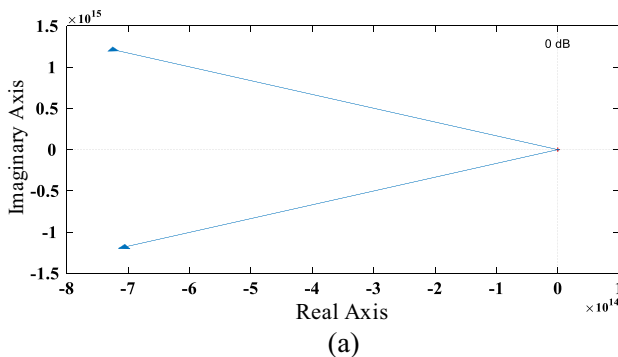


Fig. 4 a Nyquist and b root-locus plot for single-phase MG system

LQR and MPC, respectively. It is also notable that better

controller and the designed NI-RLLC controller show

Table 4 Parameters of MIMO NI-RLLC controller

Quantity	Value
Resonant gain, k_m	0.6
Resonant damping co-efficient, ζ_m	0.7
Resonant frequency, ω_m	10,300

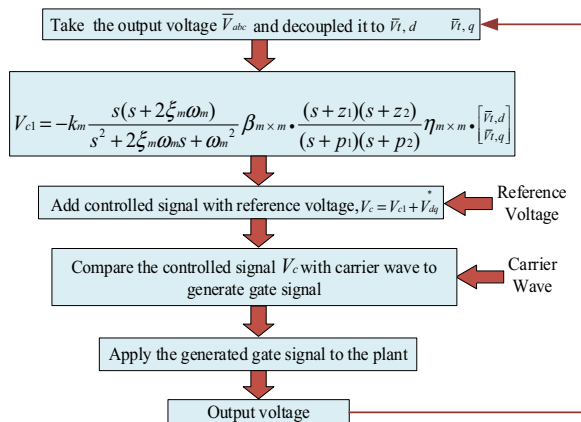
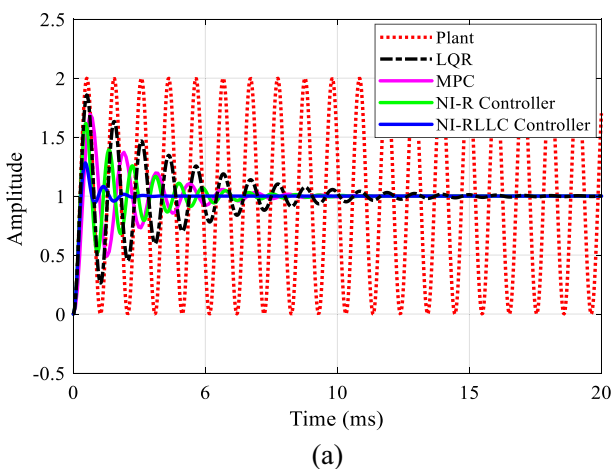


Fig. 5 Flowchart of designed NI-RLLC controller incorporating nominal plant

good performance, while the designed controller attains relatively higher damping than the NI-R controller. It is worth mentioning that the literature and previous discussions indicate that the NI-R has better responses than both MPC and LQR. Thus, it validates the claim of superior performance of the designed NI-RLLC controller over other controller designs.



5.2 Performance over changing reference value

As the prime objective of this paper is to design a controller for tracking reference voltage rigorously, the performance of this controller is verified with varying reference value. The following conditions are considered for changing reference grid voltage, V_G^* :

- $V_G^* = 200$ V; $0 < t < 0.035$ s;
- $V_G^* = 250$ V; $0.035 < t < 0.065$ s;
- $V_G^* = 150$ V; $0.065 < t < 0.1$ s;

Figure 9 verifies the robust reference tracking performance of the designed NI-RLLC controller, despite changing the reference value randomly. The NI-R controller exhibits a greater magnitude error than the designed NI-RLLC controller, and the NI-R controller shows higher oscillations during an abrupt change of reference.

5.3 Performance over some conventional loads

Commonly, an MG system deals with ranges of known and unknown loads, and their characteristics may disturb normal operation. With the aid of the designed controller, these problems can be easily addressed. To verify the effectiveness of the designed NI-RLLC controller, some common loads are modeled in Fig. 10, and a brief description of these loads is given in Table 11 in the “Appendix”.

5.3.1 Consumer load

This type of load is modeled in Fig. 10a, and improved voltage tracking of the designed NI-RLLC controller for such load is demonstrated in Fig. 11a, f. Apart from hav-

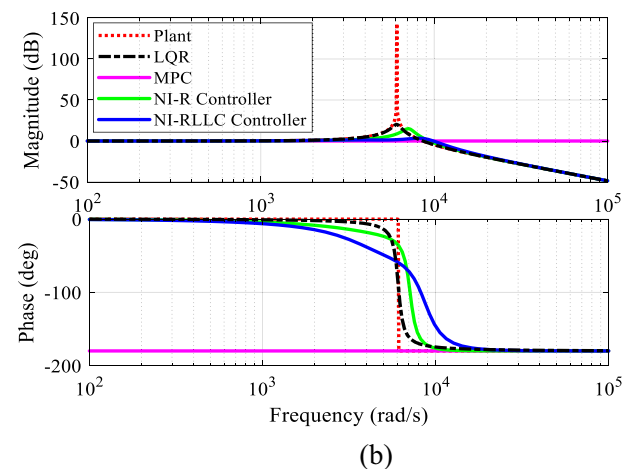


Fig. 6 Single-phase **a** step response comparison of different controllers and **b** bode plot comparison of different controllers

ing the lowest amplitude error, a higher amount of active

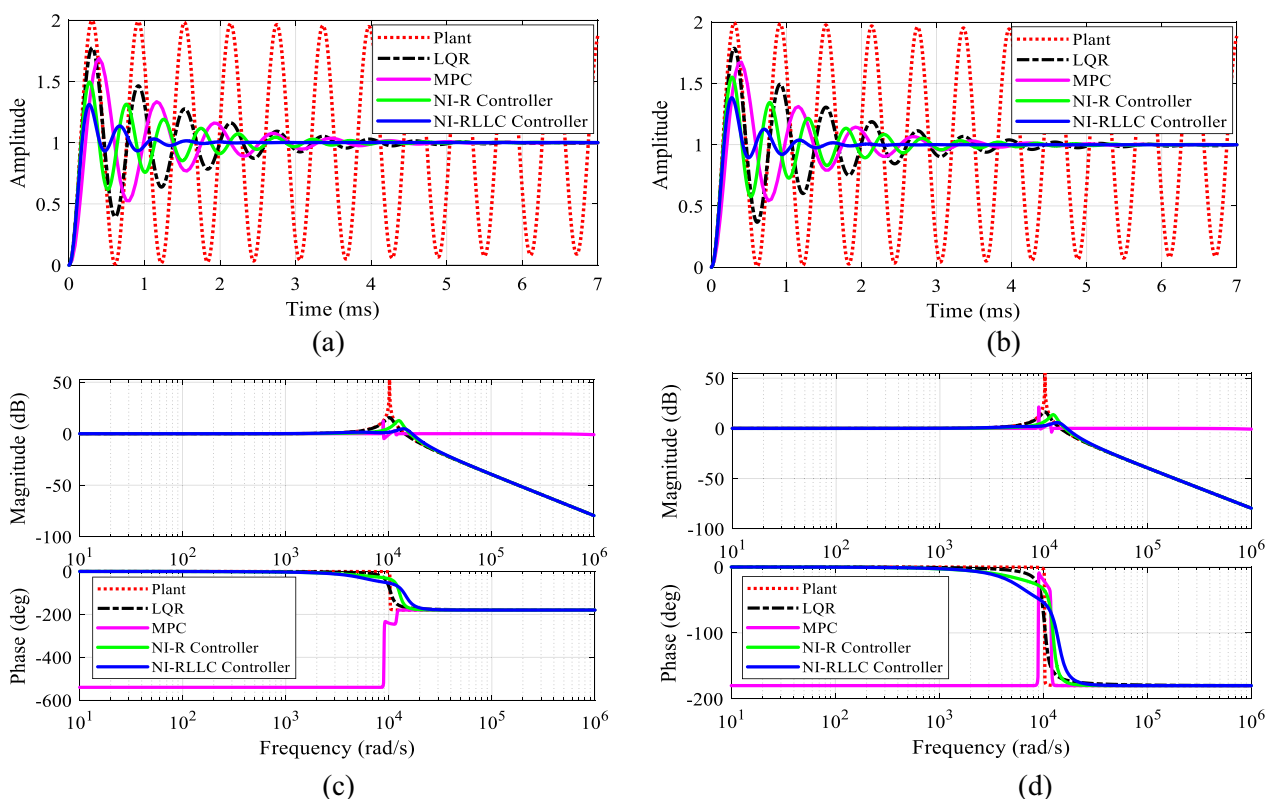


Fig. 7 Three-phase step response comparison for different controllers for **a** *d*-axis and **b** *q*-axis; bode plot comparison for different controllers for **c** *d*-axis and **d** *q*-axis

Table 5 Step response comparison of different controllers for single-phase

Controller name	Rise time (ms)	Peak time (ms)	Percentage overshoot	Settling time (ms)
NI-RLLC controller	0.197	0.460	28.09	1.7
NI-R controller	0.176	0.470	61.53	7.2
LQR	0.178	0.516	85.94	13
MPC	0.241	0.640	69.21	7.6

power is evolved using NI-RLLC controller as shown in Fig. 11k.

5.3.2 Harmonic load

Harmonics originate because of different nonlinear loads such as semiconductor devices, switching elements etc. These loads are the prime reason of over-heating of motors, cables, and capacitors etc. In order to simulate the effects of harmonic loads, they are modeled as shown in Fig. 10b. The open-loop and NI-R controller in Fig. 11b, g show more transient oscillations, but

Table 6 Step response comparison of different controllers for three-phase

Controller name	Rise time (ms)	Peak time (ms)	Percentage overshoot	Settling time (ms)
(a) <i>d</i>-axis output				
NI-RLLC controller	0.115	0.260	30.86	1.4
NI-R controller	0.107	0.266	49.17	3.5
LQR	0.108	0.301	77.66	4.3
MPC	0.143	0.400	68.66	3.9
(b) <i>q</i>-axis output				
NI-RLLC controller	0.112	0.272	38.34	1.4
NI-R controller	0.105	0.278	55.14	3.8
LQR	0.107	0.301	79.46	4.9
MPC	0.140	0.400	67.24	3.9

the designed NI-RLLC controller mitigates the oscillations and tracks the voltage waveform more accurately with fewer harmonics. It is apparent from Fig. 11l that the open-loop can extract a very low amount of power, while NI-R improves this problem significantly, but the

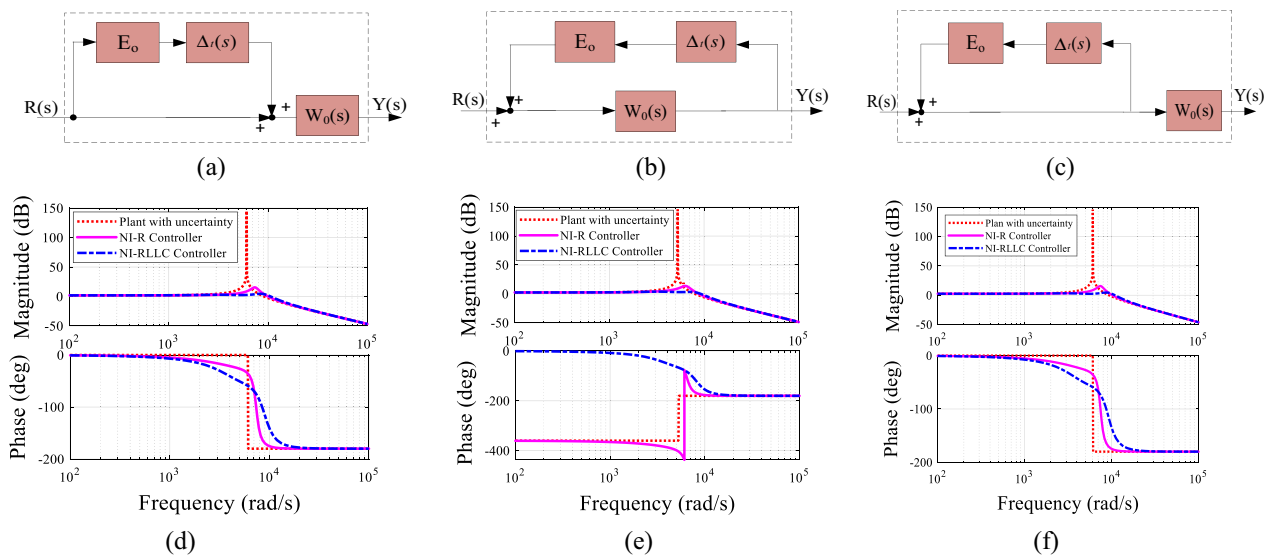


Fig. 8 Block diagram of **a** multiplicative input uncertainty **b** inverse additive uncertainty and **c** inverse multiplicative input uncertainty for single-phase MG system. Bode plot of **d** multiplicative input uncertainty **e** inverse additive uncertainty and **f** inverse multiplicative input uncertainty for single-phase MG system

designed NI-RLLC has the highest power extraction capability.

5.3.3 Unknown load

Modeling of an unknown load is shown in Fig. 10c, while open-loop, NI-R and NI-RLLC controller responses for this type of load are reported in Fig. 11c, h. It is seen that the designed NI-RLLC controller tracks the voltage most effectively with least tracking error despite changing load dynamics. In correspondence to least magnitude error, a comparatively higher amount of power is derived for the NI-RLLC controller as shown in Fig. 11m.

5.3.4 Nonlinear load

Often an MG system faces nonlinear loads, e.g., rectifiers, semiconductor devices, computers, printers, electronic lighting ballasts etc. For simulation purposes and

simple representation, this type of load is configured as shown in Fig. 10d. Figure 11d, i show that the NI-R controller performs better than the open-loop system but exhibits some phase shift in voltage tracking. However, the designed NI-RLLC controller diminishes the harmonics to a greater extent and has better voltage tracking capability than the others. In terms of power extraction, the designed NI-RLLC controller also indicates the best performance as can be seen from Fig. 11n.

5.3.5 Dynamic load

Dynamic loads as configured in Fig. 10e have considerable effects on an MG system. Large transient oscillations in voltage waveform are noted for the open-loop and NI-R controller, while the designed NI-RLLC controller effectively mitigates these oscillations and tracks the reference voltage with near zero tracking error, as shown in

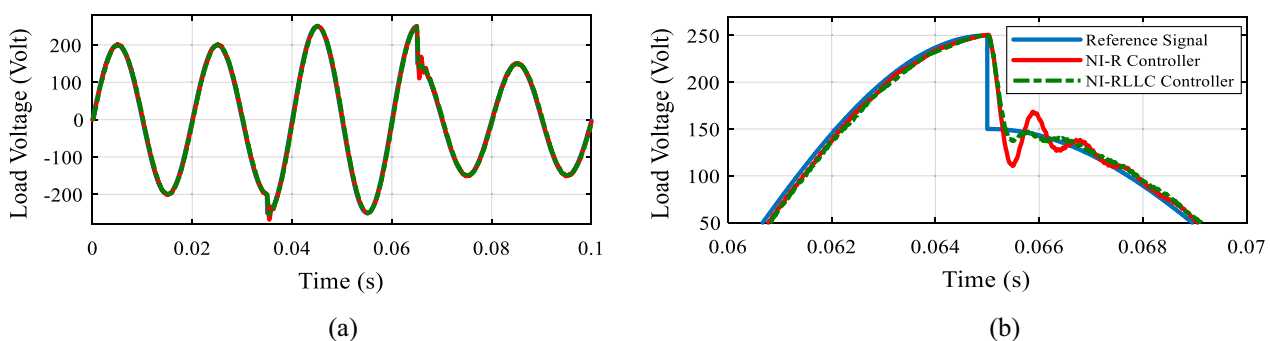


Fig. 9 Performance check for changing reference value **a** normal view **b** zoomed view

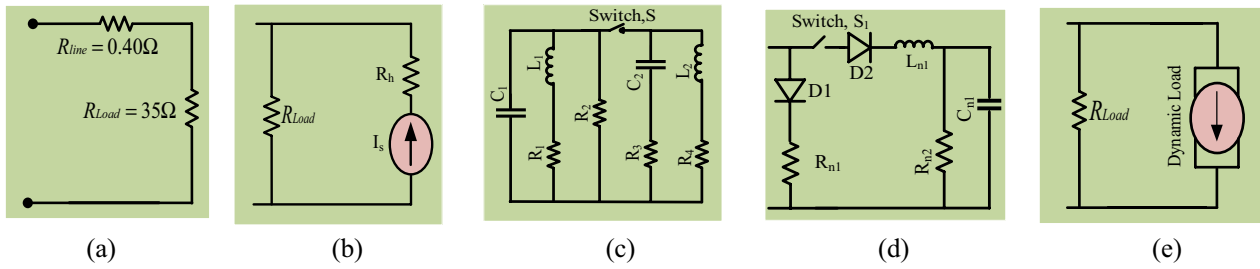


Fig. 10 Block diagram of single-phase **a** consumer load, **b** harmonic load, **c** unknown load, **d** nonlinear load, **e** dynamic load

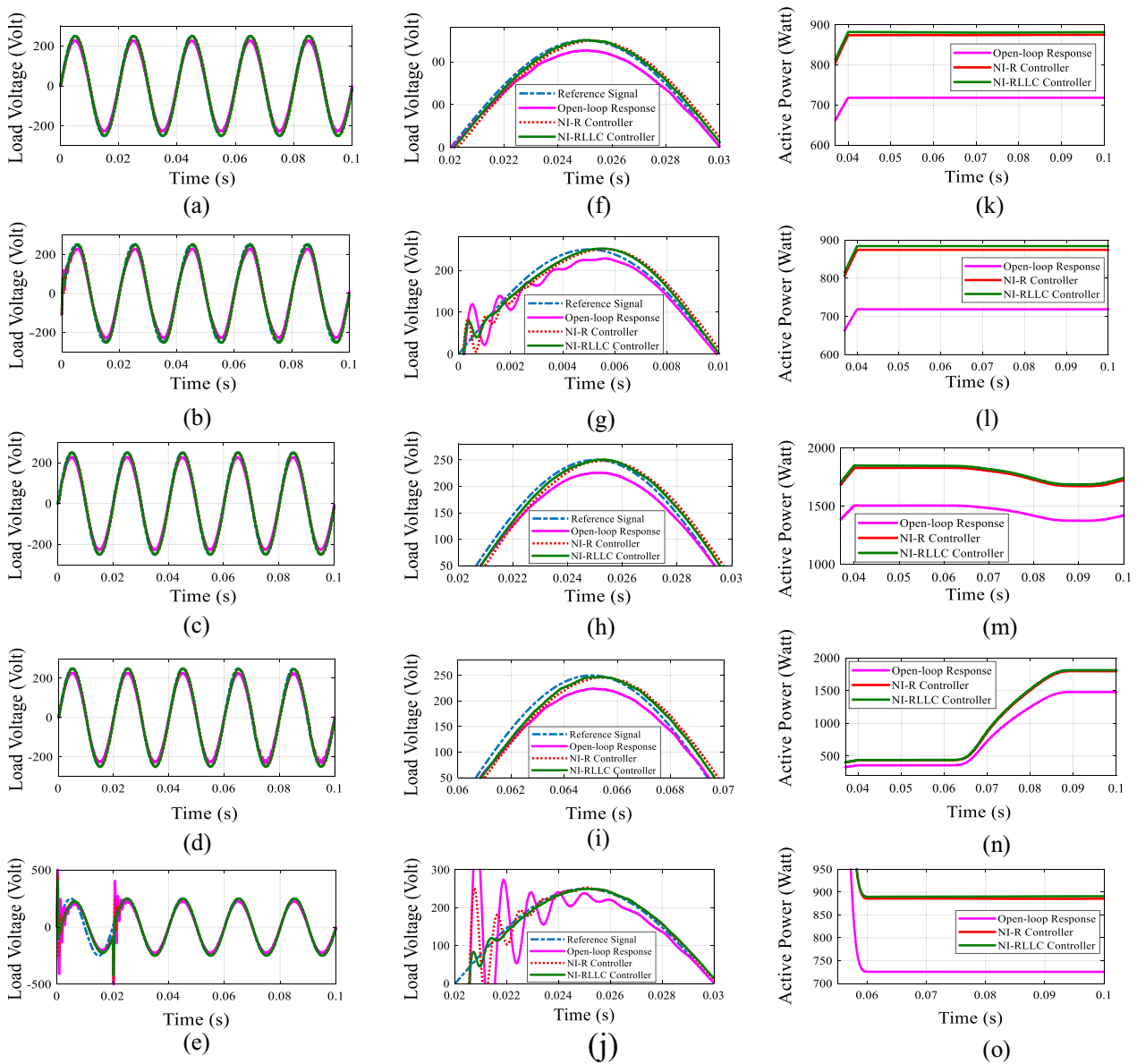


Fig. 11 Single-phase load voltage comparison of load **a** consumer, **b** harmonic, **c** unknown, **d** nonlinear, **e** dynamic. Zoomed view of load voltage of load **f** consumer, **g** harmonic, **h** unknown, **i** nonlinear, and **j** dynamic. Active power measurement of load **k** consumer, **l** harmonic, **m** unknown, **n** nonlinear and **o** dynamic

Table 7 Total harmonic distortion (THD) for different loads of SISO system

Controller name	Consumer load	Harmonic load	Unknown load	Nonlinear load	Dynamic load
NI-RLLC controller	0.59	4.84	0.70	2.09	20.93
NI-R controller	0.63	5.43	0.72	2.18	25.35
Open-loop system	0.82	6.89	1.07	2.65	36.80

Table 8 RMS voltage error for different loads of SISO system

Controller name	Consumer load	Harmonic load	Unknown load	Nonlinear load	Dynamic load
NI-RLLC controller	0.10	0.30	0.10	0.90	0.10
NI-R controller	0.20	0.40	0.30	1.00	0.70
Open-loop system	17.4	17.1	17.5	18.1	17.4

Table 9 Active power (watt) measurement for different loads of SISO system

Controller name	Consumer load	Harmonic load	Unknown load	Nonlinear load	Dynamic load
NI-RLLC controller	881.4	883.9	1743	1815	890.9
NI-R controller	878.7	877.7	1739	1809	884.5
Open-loop system	717.9	718.7	1420	1478	725.5

Fig. 11e, j. Moreover, relatively higher active power is also obtained for the designed NI-RLLC controller as shown in Fig. 11o.

5.4 Quantitative analysis of simulation performances

Quantitative analysis for the open-loop system, NI-R and NI-RLLC controllers is carried out with different loads. The THD analysis, and errors of RMS voltage and active power are investigated based on Fig. 11, and are presented in Tables 7, 8 and 9, respectively. Table 7 indicates that the lowest THD are obtained for all kinds of loads with the designed NI-RLLC controller. This is followed by the NI-R controller. In the case of RMS voltage error, the designed NI-RLLC controller minimizes the error noticeably for all loads. Taking the average RMS voltage error, a maximum error of 17.5 V is found for the open loop system, followed by 0.52 V for NI-R controller

and 0.30 V for the NI-RLLC controller. It is clear from Table 9 that the highest active power is extracted by the NI-RLLC controller under all types of loads. On average, 1242.84 W active power is extracted with the designed NI-RLLC controller. This is 5.06 W and 230.82 W higher than the NI-R controller and the open-loop system, respectively. These results demonstrate that the NI-RLLC controller has better performance under various load conditions than the others.

5.5 Performance evaluation for three-phase MG system

Simulation performance of the designed MIMO NI-RLLC controller is examined by imposing various types of three-phase loads, whose details are noted in Table 12 in the “Appendix”. Among different types of loads, consumer load is the most common form of load as depicted in Fig. 12a. The closed-loop with the NI-RLLC controller and open-loop system responses are presented in Fig. 12e, i, respectively. These indicate that the closed-loop system performs much better than the open-loop system by keeping the load voltage within the desired 1 pu value, while the open-loop system has a voltage profile of around 2 pu.

After connecting the nonlinear load as shown in Fig. 12b to the MG system, the NI-RLLC controller keeps the load voltage stable and helps it return to its normal state (1 pu) within a minimum time period as shown in Fig. 12f. On the other hand, the output voltage moves from the desirable load level because of the insertion of nonlinear load as shown in Fig. 12j.

The unknown load for a three-phase system is modeled in Fig. 12c, and the consequence of such load is shown in Fig. 12g, k for closed-loop and open-loop systems, respectively. The NI-RLLC controller shows a desirable response against this changing load dynamics by maintaining the load voltage to the level of 1 pu, but the open-loop system cannot meet the requirement at all.

In order to investigate the performance of the NI-RLLC controller during unbalanced condition, an unbalanced load is modeled as shown in Fig. 12d. Because of the control action of the NI-RLLC controller, imbalance among phases is controlled rigidly, while the open loop system fails to minimize the effects of unbalanced load as is clearly visible in Fig. 12h, l. Therefore, the desired level of load voltage is obtained for closed-loop, but the open-loop system completely loses its control after connecting the unbalanced load.

5.6 Power quality constraint measurement

Some power quality constraints, such as THD, voltage deviation and voltage imbalance ratio are considered in order to justify the use of the MIMO NI-RLLC controller. For the steady-state condition, numerical values

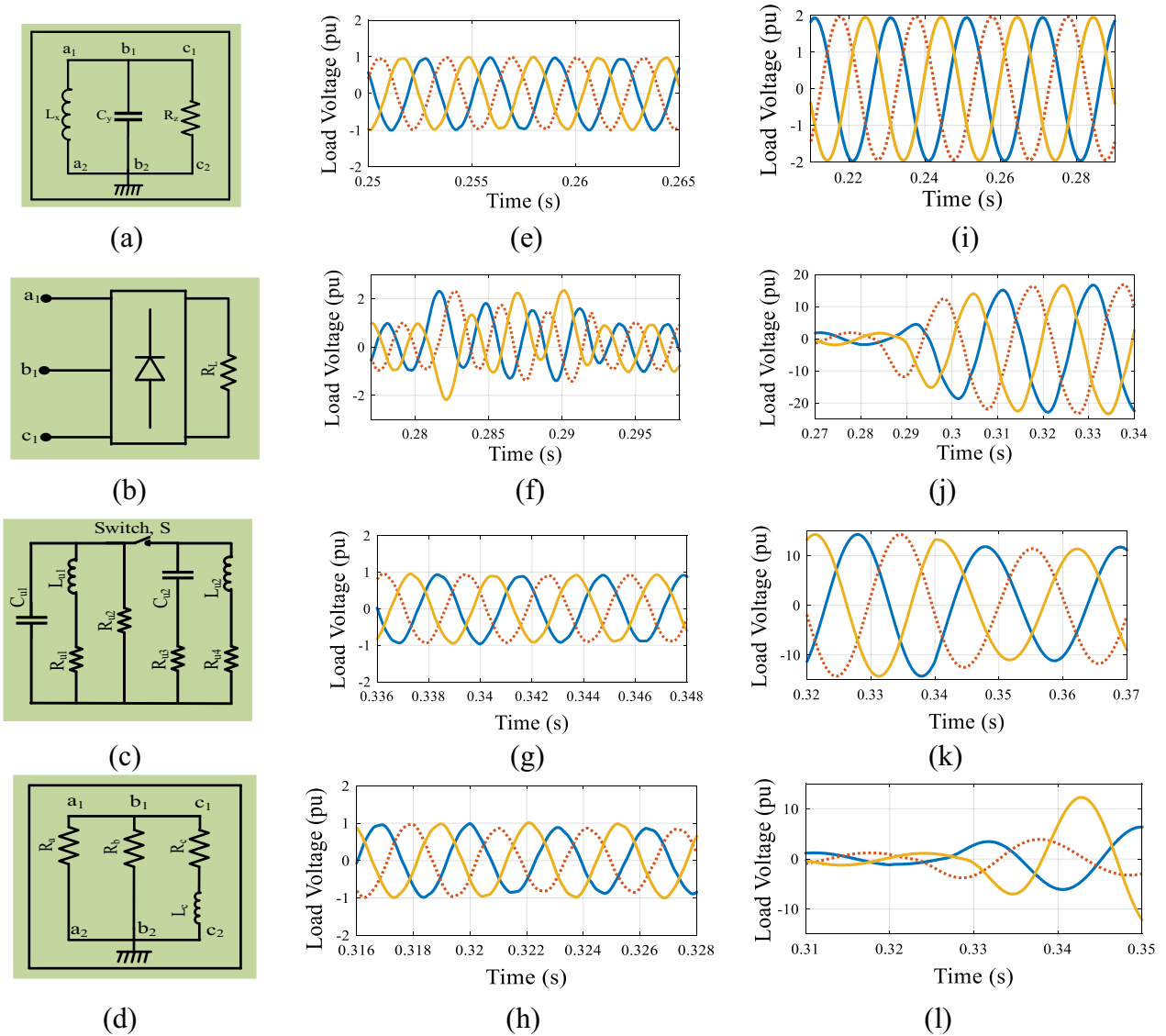


Fig. 12 Block diagram of three-phase load **a** consumer, **b** nonlinear, **c** unknown, **d** unbalanced. Three-phase load voltage for closed-loop with MIMO NI-RLLC controller for load **e** consumer, **f** nonlinear, **g** unknown, **h** unbalanced. Open-loop load voltage response of load **i** consumer, **j** nonlinear, **k** unknown and **l** unbalanced

Table 10 Power quality constraints measurement with the designed MIMO NI-RLLC controller

Types of load	Total harmonic distortion (THD) [standard: < 5%]	Voltage deviation [standard: < 5%]	Voltage imbalance ratio [standard: < 3%]
Consumer load	2.00	1.02	0.00
Nonlinear load	2.12	2.97	2.87
Unknown load	2.06	3.02	0.00
Unbalanced load	2.19	4.53	2.79

are measured for various loads and listed in Table 10. It is clear that all the measured values satisfy the standard IEEE Std-1547 [50]. This affirms the robust performance of this NI-RLLC controller for three-phase MG technology.

6 Conclusion

This paper presents a lead-lag compensator conjugated resonant controller, designed by following the negative imaginary theorem, abbreviated as NI-RLLC controller for both single-phase and three-phase autonomous MG systems. The efficacy of the proposed controller is proven by comparing its performance with LQR, MPC and NI-R controllers and open-loop response. From the simulation results and numerical analysis, the following can be stated:

- Step response and bode plots confirm that the designed NI-RLLC controller has better responses than the LQR, MPC and NI-R controller for both single-phase and three-phase MG systems. Furthermore, the Nyquist plot and root-locus indicate that system stability is guaranteed.

- The NI-RLLC controller attains 139.64 dB damping which is 11.74 dB higher than its closest competitor, i.e., NI-R controller. In addition, 722 rad/s higher bandwidth is obtained for the NI-RLLC controller than the NI-R controller.
- The NI-RLLC controller maintains its superiority for different uncertainties and for continuously changing reference value.
- For a SISO system, the NI-RLLC controller has the best performance in terms of THD and RMS voltage error, while it also has the capability to extract the highest amount of active power for several types of loads. Similarly, for the MIMO system, the NI-RLLC controller maintains all power quality constraints within the IEEE Std-1547 standard.
- For both SISO and MIMO, the proposed NI-RLLC controllers have the best voltage tracking capability for different load dynamics.

Appendix

See Tables 11 and 12.

Table 11 Parameters of single-phase load

Types of load	Load description
Consumer load	$R_{Load} = 35\Omega, R_{line} = .40\Omega$
Harmonic Load	Current source, $I_s = 7$ A, 150 Hz $R_n = 30\Omega, R_{Load} = 35\Omega$
Unknown load	$C_1 = 40 \mu F, R_1 = .40\Omega, L_1 = 215$ mH, $R_2 = 40\Omega$, and after $t = 0.06$ s, added $R_3 = 80\Omega, C_2 = 12 \mu F, R_4 = 160\Omega, L_2 = 110 \mu H$
Nonlinear load	Diode $D_1, R_{n1} = 35\Omega$, after $t = 0.06$ s, added diode $D_2, L_{n1} = 8.4$ mH, $R_{n2} = 10\Omega, C_{n1} = 15 \mu F$
Dynamic load	60 MW and 30 MVAR (steady-state voltage 60 V)

Table 12 Parameters of three-phase load

Types of load	Load description
Consumer load	$L_x = 106$ mH, $C_y = 1.2$ pF, $R_z = 4.5\Omega$
Nonlinear load	Six pulse four diode bridge rectifier, $R_L = 4.5\Omega$
Unknown load	$C_{u1} = 7 \mu F, R_{u1} = 4.30\Omega, L_{u1} = 230$ mH, $R_{u2} = 225\Omega$, and after $t = 0.34$ s, added $R_{u3} = 80\Omega, C_{u2} = 10\mu F, R_{u4} = 160\Omega, L_{u2} = 110$ mH
Unbalanced load	$R_a = 50\Omega, R_b = 35\Omega, R_c = 20\Omega$ and $L_c = 100$ mH

Abbreviations

MG: Microgrid; NI: Negative imaginary; PV: Photovoltaic; DG: Distributed generator; ESS: Energy storage system; VSI: Voltage source inverter; LQR: Linear quadratic regulator; I-LQR: Integral linear quadratic regulator; LQG: Linear quadratic Gaussian; I-LQG: Integral linear quadratic Gaussian; PID: Proportional integral derivative; PI: Proportional integral; DSP: Digital signal processing; MPC: Model predictive control; THD: Total harmonic distortion; PWM: Pulse width modulation; P-RC: Proportional resonant controller; PI-RC: Proportional integral resonant controller; NI-R: Negative imaginary resonant; LLC: Lead-lag compensator; NI-RLLC: Negative imaginary resonant lead-lag compensator; PCC: Point of common coupling; IGBT: Insulated gate bipolar transistor; SISO: Single input single output; MIMO: Multiple input multiple output; RMS: Root mean square.

Acknowledgements

Not applicable.

Authors' contributions

Conceptualization, MYYUH and MRI; methodology, MYYUH and MRI; software, MYYUH; validation, MRI, TA and MRIS; formal analysis, MYYUH and MRI; writing—original draft, MYYUH; writing—review and editing, MRI, TA and MRIS; supervision, TA and MRIS. All the authors read and approved the final manuscript.

Authors' information

Md. Yah-Ya Ul Haque received his B.Sc. degree in Electrical and Electronic Engineering from Rajshahi University of Engineering & Technology (RUET). Currently, he is working as a Lecturer with the Department of EEE, Varendra University, Rajshahi. His research interests are renewable energy, power electronics, power system protection and control engineering.

Md. Rashidul Islam received the B.Sc. and M.Sc. degrees in electrical and electronic engineering (EEE) from the Rajshahi University of Engineering and Technology (RUET), Rajshahi, Bangladesh, in 2013 and 2017, respectively. He was a Lecturer with the Department of EEE, Varendra University, Rajshahi. He is currently working as an Assistant Professor with the Department of EEE, RUET. His research interests include nonlinear controller design and applications on renewable energy systems, the applications of power electronics in renewable energy, microgrid systems, and fault ride through capability augmentation. He received the University Gold Medal Award from the RUET. He also received the Prime Minister Gold Medal Award.

Tanvir Ahmed received the B.Sc. and M.Sc. degrees in electrical and electronic engineering from the Rajshahi University of Engineering and Technology (RUET), Rajshahi, Bangladesh, in 2009, and 2012, respectively, and the Ph.D. degree in electrical and information engineering from the University of Sydney, Australia, in 2017. Upon completion of the B.Sc. degree, he joined in electrical and electronic engineering department, RUET, where he is currently a Professor. His research interests include nonlinear optics, optical device, and optical communication.

Md. Rafiqul Islam Sheikh was born in Sirajgonj, Bangladesh, in October 1967. He received the B.Sc. (Eng.) and M.Sc. (Eng.) degrees from the Rajshahi University of Engineering & Technology (RUET), Bangladesh, in 1992 and 2003, respectively, and the Ph.D. degree from the Kitami Institute of Technology, Hokkaido, Kitami, Japan, in 2010, all in electrical and electronic engineering (EEE). He joined as a Lecturer with the EEE Department, RUET, in 1994, where he is currently a Professor. He is also working as a Vice Chancellor with RUET. His research interests are, power system stability enhancement by using FACTS devices, renewable energy technologies, smart grid, and load frequency control of multi-area power systems. He has published many technical journal and conference papers, and authored or coauthored three books, and three book chapters. Dr. Sheikh is the Fellow IEB and the member of BCS Bangladesh.

Funding

This work is carried out without the support of any funding agency.

Availability of data and materials

Please contact author for data material request.

Declarations

Competing interests

The authors declare that they have no known competing financial interests or personal relationships that could have appeared to influence the work reported in this paper.

Author details

¹Department of Electrical and Electronic Engineering, Varendra University, Rajshahi 6204, Bangladesh. ²Department of Electrical and Electronic Engineering, Rajshahi University of Engineering & Technology, Rajshahi 6204, Bangladesh.

Received: 30 September 2020 Accepted: 20 February 2022

Published online: 10 March 2022

References

- Moorthy, K., Patwa, N., Gupta, Y., et al. (2019). Breaking barriers in deployment of renewable energy. *Heliyon*, 5(1), e01166.
- Islam, M., Huda, M., Hasan, J., Sadi, M. A. H., Abu Hussein, A., Roy, T. K., Mahmud, M., et al. (2020). Fault ride through capability improvement of dfig based wind farm using nonlinear controller based bridge-type flux coupling non-superconducting fault current limiter. *Energies*, 13(7), 1696.
- Hu, B., Wang, H., & Yao, S. (2017). Optimal economic operation of isolated community microgrid incorporating temperature controlling devices. *Protection and Control of Modern Power Systems*, 2(1), 6.
- Islam, M. R., Hasan, J., Shipon, M. R. R., Sadi, M. A. H., Abu Hussein, A., & Roy, T. K. (2020). Neuro fuzzy logic controlled parallel resonance type fault current limiter to improve the fault ride through capability of dfig based wind farm. *IEEE Access*, 8, 115314–115334.
- Olivares, D. E., Mehrizi-Sani, A., Etemadi, A. H., Canizares, C. A., Iravani, R., Kazerani, M., Hajimiragha, A. H., Gomis-Bellmunt, O., Saeedifard, M., Palma-Behnke, R., et al. (2014). Trends in microgrid control. *IEEE Transactions on Smart Grid*, 5(4), 1905–1919.
- Islam, M. R., Hasan, J., Shipon, M. R., Huda, M. N., Sadi, M. A. H., & Abu Hussein, A. (2021). Performance improvement of dfig based wind farms using narma-12 controlled bridge-type flux coupling non-superconducting fault current limiter. *IET Generation, Transmission & Distribution*, 14(26), 6580–6593.
- Iqbal, F., & Siddiqui, A. S. (2017). Optimal configuration analysis for a campus microgrid—A case study. *Protection and Control of Modern Power Systems*, 2(1), 23.
- Lopes, J. P., Moreira, C., & Madureira, A. (2006). Defining control strategies for microgrids islanded operation. *IEEE Transactions on Power Systems*, 21(2), 916–924.
- Andishgar, M. H., Gholipour, E., & Hooshmand, R.-A. (2017). An overview of control approaches of inverter-based microgrids in islanding mode of operation. *Renewable and Sustainable Energy Reviews*, 80, 1043–1060.
- Patarroyo-Montenegro, J. F., Salazar-Duque, J. E., & Andrade, F. (2018). Lqr controller with optimal reference tracking for inverter-based generators on islanded-mode microgrids. In *IEEE ANDESCON* (pp. 1–5). IEEE.
- Tran, T. V., Yoon, S.-J., & Kim, K.-H. (2018). An lqr-based controller design for an lcl-filtered grid-connected inverter in discrete-time state-space under distorted grid environment. *Energies*, 11(8), 2062.
- Al Hassan, H. A., Alharbi, T., Morello, S. A., Mac, Z.-H., & Grainger, B. M. (2018). Linear quadratic integral voltage control of islanded ac microgrid under large load changes. In *9th IEEE international symposium on power electronics for distributed generation systems (PEDG)* (pp. 1–5). IEEE.
- Andani, M. T., Pourgharibshahi, H., Ramezani, Z., & Zargarzadeh, H. (2018). Controller design for voltage-source converter using lqg/ltr. In *IEEE Texas power and energy conference (TPEC)* (pp. 1–6). IEEE.
- Islam, M. R., Hasan, M. M., Badal, F. R., Das, S. K., & Ghosh, S. K. (2020). A blended improved h5 topology with ilqg controller to augment the performance of microgrid system for grid-connected operations. *IEEE Access*, 8, 69639–69660.
- Alhamrouni, I., Hairullah, M., Omar, N., Salem, M., Jusoh, A., & Sutikno, T. (2019). Modelling and design of pid controller for voltage control of

- ac hybrid micro-grid. *International Journal of Power Electronics and Drive Systems*, 10(1), 151.
16. Hossain, M. A., & Pota, H. R. (2015). Voltage tracking of a single-phase inverter in an islanded microgrid. *International Journal of Renewable Energy Research (IJRER)*, 5(3), 806–814.
 17. Firuzi, M. F., Roosta, A., & Gitzadeh, M. (2019). Stability analysis and decentralized control of inverter-based ac microgrid. *Protection and Control of Modern Power Systems*, 4(1), 1–24.
 18. Awal, M., Yu, H., Tu, H., Lukic, S. M., & Husain, I. (2019). Hierarchical control for virtual oscillator based grid-connected and islanded microgrids. *IEEE Transactions on Power Electronics*, 35(1), 988–1001.
 19. Kabalci, E. (2020). Hierarchical control in microgrid. In *Microgrid architectures, control and protection methods* (pp. 381–401). Springer.
 20. Sheela, A., Vijayachitra, S., & Revathi, S. (2015). H-infinity controller for frequency and voltage regulation in grid-connected and islanded microgrid. *IEEJ Transactions on Electrical and Electronic Engineering*, 10(5), 503–511.
 21. Jankovic, Z., Nasiri, A., & Wei, L. (2015). Robust h-infinity controller design for microgrid-tied inverter applications. In *IEEE Energy Conversion Congress and Exposition (ECCE)* (pp. 2368–2373). IEEE.
 22. Palizban, O., & Kauhaniemi, K. (2015). Hierarchical control structure in microgrids with distributed generation: Island and grid-connected mode. *Renewable and Sustainable Energy Reviews*, 44, 797–813.
 23. Feng, X., Shekhar, A., Yang, F., Hebnner, R. E., & Bauer, P. (2017). Comparison of hierarchical control and distributed control for microgrid. *Electric Power Components and Systems*, 45(10), 1043–1056.
 24. Dragičević, T. (2017). Model predictive control of power converters for robust and fast operation of ac microgrids. *IEEE Transactions on Power Electronics*, 33(7), 6304–6317.
 25. Shan, Y., Hu, J., Li, Z., & Guerrero, J. M. (2018). A model predictive control for renewable energy based ac microgrids without any pid regulators. *IEEE Transactions on Power Electronics*, 33(11), 9122–9126.
 26. Prasad, V., Jayasree, P., & Sruthy, V. (2016). Hysteresis current controller for a micro-grid application. In *International conference on energy efficient technologies for sustainability (ICEETS)*, pp. 73–77. IEEE.
 27. Putri, A. I., Rizqiawan, A., Rozzi, F., Zakkia, N., Haroen, Y., & Dahono, P. A. (2016). A hysteresis current controller for grid-connected inverter with reduced losses. In *2nd International conference of industrial, mechanical, electrical, and chemical engineering (ICIMECE)* (pp. 167–170). IEEE.
 28. Trivedi, A., & Singh, M. (2016). Repetitive controller for vsis in droop based ac-microgrid. *IEEE Transactions on Power Electronics*, 32(8), 6595–6604.
 29. Ma, W., & Ouyang, S. (2019). Control strategy for inverters in microgrid based on repetitive and state feedback control. *International Journal of Electrical Power & Energy Systems*, 111, 447–458.
 30. Padula, A. S., Agnoletto, E. J., Neves, R. V., Magossi, R. F., Machado, R. Q., & Oliveira, V. A. (2019). Partial harmonic current distortion mitigation in microgrids using proportional resonant controller. In *18th European control conference (ECC)* (pp. 435–440). IEEE.
 31. Wang, X., Blaabjerg, F., & Chen, Z. (2013). Autonomous control of inverter-interfaced distributed generation units for harmonic current filtering and resonance damping in an islanded microgrid. *IEEE Transactions on Industry Applications*, 50(1), 452–461.
 32. Lopez-Nuñez, A. R., Mina, J. D., Aguayo, J., & Calderon, G. (2016). Proportional integral resonant controller for current harmonics mitigation in a wind energy conversion system. In *13th International conference on power electronics (CIEP)* (pp. 232–237). IEEE.
 33. Sarkar, S. K., Roni, M. H. K., Datta, D., Das, S. K., & Pota, H. R. (2018). Improved design of high-performance controller for voltage control of islanded microgrid. *IEEE Systems Journal*, 13(2), 1786–1795.
 34. Haque, M.Y.-Y.U., Islam, M. R., Hasan, J., & Sheikh, M. R. I. (2021). Negative imaginary theory-based proportional resonant controller for voltage control of three-phase islanded microgrid. *Journal of Control, Automation and Electrical Systems*, 32(1), 214–226.
 35. Rahman, M. M., Biswas, S. P., Hosain, M. K., & Sheikh, M. R. I. (2019). A second order high performance resonant controller for single phase islanded microgrid. In *4th International conference on electrical information and communication technology (EICT)* (pp. 1–6). IEEE.
 36. Vandoorn, T. L., De Kooning, J. D., Meersman, B., & Zwaenepoel, B. (2015). Control of storage elements in an islanded microgrid with voltage-based control of dg units and loads. *International Journal of Electrical Power & Energy Systems*, 64, 996–1006.
 37. Cai, H., Wei, W., Peng, Y., & Hu, H. (2014). Fuzzy proportional-resonant control strategy for three-phase inverters in islanded micro-grid with nonlinear loads. In *IEEE international conference on fuzzy systems (FUZZ-IEEE)* (pp. 707–712). IEEE.
 38. Hossain, M., Pota, H., Hossain, M., & Haruni, A. (2018). Active power management in a low-voltage islanded microgrid. *International Journal of Electrical Power & Energy Systems*, 98, 36–47.
 39. Vandoorn, T. L., Ionescu, C. M., De Kooning, J. D., De Keyser, R., & Van-develde, L. (2012). Theoretical analysis and experimental validation of single-phase direct versus cascade voltage control in islanded microgrids. *IEEE Transactions on Industrial Electronics*, 60(2), 789–798.
 40. Sarker, S. K., Badal, F. R., Das, P., & Das, S. K. (2019). Multivariable integral linear quadratic gaussian robust control of islanded microgrid to mitigate voltage oscillation for improving transient response. *Asian Journal of Control*, 21(4), 2114–2125.
 41. Karimi, H., Davison, E. J., & Iravani, R. (2009). Multivariable servomechanism controller for autonomous operation of a distributed generation unit: Design and performance evaluation. *IEEE Transactions on Power Systems*, 25(2), 853–865.
 42. Hosen, M., Abir, M., Rana, M., & Ali, M. (2019). An optimal control of three phase islanded microgrid system. In *International conference on electrical, computer and communication engineering (ECCE)* (pp. 1–5). IEEE.
 43. Petersen, I. R., & Lanzon, A. (2010). Feedback control of negative imaginary systems. *IEEE Control Systems Magazine*, 30(5), 54–72.
 44. Petersen, I. R. (2016). Negative imaginary systems theory and applications. *Annual Reviews in Control*, 42, 309–318.
 45. Das, S. K., Pota, H. R., & Petersen, I. R. (2015). Multivariable negative imaginary controller design for damping and cross coupling reduction of nano positioners: A reference model matching approach. *IEEE/ASME Transactions on Mechatronics*, 20(6), 3123–3134.
 46. Verma, G., Verma, V., Jhambhulkar, S., & Verma, H. (2015). Design of a lead-lag compensator for position loop control of a gimbaled payload. In *2nd international conference on signal processing and integrated networks (SPIN)* (pp. 394–399). IEEE.
 47. Jadoon, Z. K., Shakeel, S., Saleem, A., Khaqan, A., Shuja, S., Malik, S. A., Ali Riaz, R., et al. (2017). A comparative analysis of pid, lead, lag, lead-lag, and cascaded lead controllers for a drug infusion system. *Journal of Healthcare Engineering*. <https://doi.org/10.1155/2017/3153252>
 48. Alepuz, S., Salaet, J., Gilabert, A., Bordonau, J., & Peracaula, J. (2002). Control of three-level vsis with a lqr-based gain-scheduling technique applied to dc-link neutral voltage and power regulation. In *IEEE 2002 28th Annual Conference of the Industrial Electronics Society. IECON 02* (Vol. 2, pp. 914–919). IEEE.
 49. Wang, L. (2009). *Model predictive control system design and implementation using MATLAB®*. Springer.
 50. Photovoltaics, D. G., & Storage, E. (2009). IEEE application guide for IEEE STD 1547™, IEEE standard for interconnecting distributed resources with electric power systems.

Publisher's Note

Springer Nature remains neutral with regard to jurisdictional claims in published maps and institutional affiliations.